Quantum size effects in optical properties of CdS-glass composites

Barrett G. Potter, Jr. and Joseph H. Simmons
University of Florida, Gainesville, Florida 32611
(Received 9 November 1987)

The optical properties of extremely small isolated semiconductors provide a sensitive probe of the developing electronic structure in the materials. Cadmium sulfide and CdS_xSe_{1-x} crystallites are precipitated in an insulating glass matrix during a secondary heat-treatment procedure. Variation in the heat treatment significantly alters the final crystallite size, enabling the examination of a size-dependent change in the observed optical-absorption edge and exciton-related photoluminescence peak energies. A diffusion-limited coarsening behavior is exhibited by the CdS crystallites precipitated from a Zn-free base glass, indicating a high degree of purity in these crystals. Growth behavior of mixed crystallites, however, indicates some stoichiometric variation with heat-treatment time. Quantum size effects measured using the CdS precipitates in the size range from 40–400 Å reflect confinement primarily in the translational motion of the Wannier exciton with some slight modification of its internal electron and hole orbits.

INTRODUCTION

The optical behavior of quantum size semiconductors promises to provide a sensitive probe for the effect of quantum confinement of the electron and hole wave functions by a deep potential well on the excitonic and band-gap energy structures. Recently, several groups have conducted experimental and theoretical studies of the optical behavior of confined Wannier excitons in CdS, CuCl, CdSe, and CdS_xSe_{1-x} in the form of precipitated colloids in solution or crystals in glass, or doped alkali-halide crystal matrices. In the theoretical studies, limiting cases of very large and very small crystals with respect to Bohr orbit radii for the electron and hole have been treated in closed form and variational approaches have begun to resolve the intermediate-size cases. The experimental studies, however, as will be shown below, have been plagued with either a lack of variation of microstructure size, or an inability to separate quantum size effects from the effects of changes in the stoichiometry of the precipitated crystals.

In this paper, we consider semiconductor-glass composites containing both CdS and CdS_xSe_{1-x} with the goal of characterizing the optical-property changes resulting from variations in the crystal size, and relating these changes to the quantum size effects on the electron-hole pairs discussed in the theoretical analyses. We will show that when studying quantum size effects, only the composites containing pure CdS crystals can be used because of the inability to control crystal composition or stoichiometry variations occurring with the size variations in composites having mixed crystals or having matrix components which can mix with the semiconductors. We will give indirect evidence supporting the appearance of uncontrolled stoichiometry variations in heat treatments of mixed crystal CdS_xSe_{1-x} composites with glass.

Warnock and Awschalom,[1,2] using several CdS_xSe_{1-x}-doped Corning filter glasses of different glass compositions, show a variation in photoluminescence peak energy position which appears to correspond to estimated differences in crystal size, shifting to higher energies with smaller average crystallite sizes [measured using transmission electron microscopy (TEM)]. They attribute this effect to the quantum confinement of the corresponding electronic state responsible for the luminescence peak, in this case identified as being the bound exciton existing within the band gap of the crystallites.

Subsequent work on identical compositions by Borrelli *et al.*[3] revealed that the crystallite sizes in these glasses are significantly larger than would be appropriate to achieve energy-state shifts of the order observed by Warnock and Awschalom. Furthermore, x-ray diffraction data presented by Borrelli *et al.* suggest that the peak shifts observed by the previous researchers originate from crystallite stoichiometry differences between the samples of different glass compositions.

To eliminate the competing crystal stoichiometry effect from the confinement-induced shift in optical properties, Borrelli *et al.*[3] performed tests on glass composites doped only with CdS. However, their base glass contains Zn which has been shown to form a substitutional solid solution with CdS, shifting the band gap to higher energies. Their x-ray diffraction data unfortunately does not allow a clear determination of the crystal stoichiometry during growth. While the authors expect that a significant amount of Zn gets into the CdS crystals in their experimental glasses at very long heat-treatment times, it is likely that some Zn alloying occurs at all heat treatments with the Zn-Cd ratio being determined by their relative diffusion coefficients.

The separation of the compositional and size-related variations in optical properties is attained by Brus[4–6] and Rossetti *et al.*[7,8] who produced CdS colloidal solutions. Here, quantum confinement effects are observed to increase the band-gap energy and shift the observed position of resonant Raman lines with a decrease in average particle size. In this case, the authors expect to have

formed pure CdS crystals, but variations in particle size are not readily feasible, therefore the functional form of the confinement effect could not be tested.

Below we show that, with proper selection of base glass and semiconductor composition, optical filter glasses can be used to study quantum confinement over a wide range of sizes free from modifications induced by changes in crystal stoichiometry. This is attained through the doping of a Zn-free base glass with CdS and heat treating to produce the desired microstructure size. Accurate crystal size measurements and a growth analysis show that the system strictly follows a pure structure-ripening model and consequently that the observed optical behavior results only from size changes in the CdS glass. In contrast, similar measurements and analysis by the structure-ripening model suggest that the optical behavior of CdS_xSe_{1-x} glass-crystal composites results from a combination of size and crystal composition changes during heat treatment.

EXPERIMENT

The glasses used in the present study were obtained in a non-heat-treated condition from Schott Glass Technologies (Duryea, PA). Two compositions were provided, one a common optical Ca crown glass doped with only Cd and S (containing SiO_2, B_2O_3, Na_2O, K_2O, and CaO) and the second, a Zn crown glass doped with Cd, S, and Se to produce a mixed crystal upon heat treatment (containing SiO_2, B_2O_3, Na_2O, K_2O, and ZnO).

Both compositions were isothermally treated from their annealed, as-received state under an air atmosphere in an electric muffle-tube furnace for time periods from 5 min to 18 h to produce a wide variation in the resulting average crystallite size. Attempts were made to minimize the width of the distribution of crystallite sizes in the CdS glass by separating the crystal-nucleation step from the growth step by a double heat-treatment procedure. Here, the CdS-doped glass was remelted at 1400 °C and then quenched between two brass plates to attempt to suppress the nucleation of the CdS microcrystals. The glass was then treated at 548 °C ($T_g + 13$ °C) for 4, 8, and 12 h to nucleate the glass prior to striking at 800 °C, where crystal growth dominates.

The resulting glass microstructures were studied by direct examination of the precipitated crystallites by AS-TEM, using C–Pt-shadowed fracture surface extraction replicas. Thus, crystallite size distribution, crystallite composition, and crystal structure could be analyzed through transmission electron microscopy, energy-dispersive x-ray analysis, and electron diffraction, respectively. However, this sampling method precludes the measurement of crystal volume fraction or any preferred orientation within the matrix, because the crystallites are collected from solution onto a carbon replica and their collective appearance on the micrographs is not representative of their relative positions in the glass matrix.

The struck samples were then subjected to both optical-absorption and photoluminescence measurements.

Absorption measurements from room temperature to 9.0 K were performed on 2-mm-thick slabs of glass in a spectrometer with an effective resolution of 4.9 meV.

Low-temperature, laser-excited photoluminescence (PL) was conducted using a 10-mW cw Ar-ion laser line at 457.9 nm. The Ar laser source was reduced to a spot size of ~ 0.1 mm on the sample with the resulting radiation focused onto the slit of a 0.33-m spectrometer utilizing an intensified photodiode array detector. Two different diffraction gratings were used to obtain resolutions of 0.95 and 14.9 Å. Additionally, a double-monochromator Raman spectrometer was employed to examine the spectral features (i.e., resonant Raman scattering) close to the laser line with a resolution of 0.56 Å.

RESULTS AND DISCUSSION

Microstructure

Figures 1 and 2 contain TEM micrographs of fracture surface replicas produced from selected CdS-doped and CdS_xSe_{1-x}-doped glass samples. These specimens were struck at their respective temperatures for 20 min. A significantly different crystallite morphology is evidenced by these two compositions which is representative of all specimens produced. The CdS_xSe_{1-x} crystallites exhibit an angular or "blocky" appearance resembling rectangles with aspect ratios approaching 2.0 to 2.2. In contrast, the CdS crystals appear more rounded in shape having a wider distribution of aspect ratios (1.0 to 2.2) at this striking time. Electron-diffraction analysis performed on samples subjected to longer striking times results in a speckled ring pattern of hexagonal symmetry. Energy-dispersive x-ray analysis provided qualitative verification of the composition of these larger crystallites.

The size of the crystallites was measured along their longest dimension yielding average sizes for the pictured specimens of 106 and 206 Å for the CdS and CdS_xSe_{1-x}-containing glasses, respectively. The standard deviation of sizes about the average is found to remain between 15 and 20 Å for the mixed crystals subjected to striking times < 1 h while the CdS glass exhibits a gradual broadening in the size distribution with heat-treatment time. After longer striking times the size distribution also broadens in the CdS_xSe_{1-x} glasses resulting in a standard deviation of ~ 40 Å while that of the pure CdS-doped glass continues to broaden, exhibiting a standard deviation $\gtrsim 80$ Å after 11 h at 800 °C. The major difference in behavior between the two glasses is seen in the time dependence of average crystal size (Fig. 3). It is precisely this effect, as discussed below, which allows the separation of growth with size change only from growth with both size and crystal stoichiometry variation.

Focusing on the pure CdS glass, a cube-root dependence of the average crystal size with heat-treatment time is found (Fig. 3). This behavior suggests that the primary growth process is a pure ripening or coarsening effect.

A coarsening of particles is generally observed in the later stages of a precipitation process after the supersaturation of the matrix with respect to the solute atoms has become sufficiently small that the nucleation of new

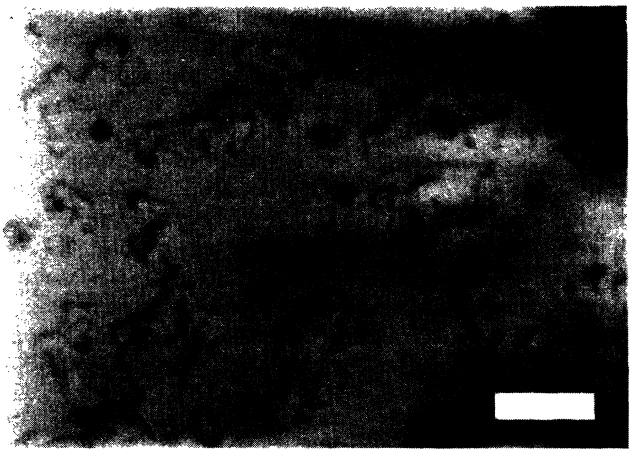

FIG. 1. Microstructure observed in TEM analysis of a CdS-glass composite subjected to a 20-min heat treatment at 800 °C (the bar represents 0.1 μm).

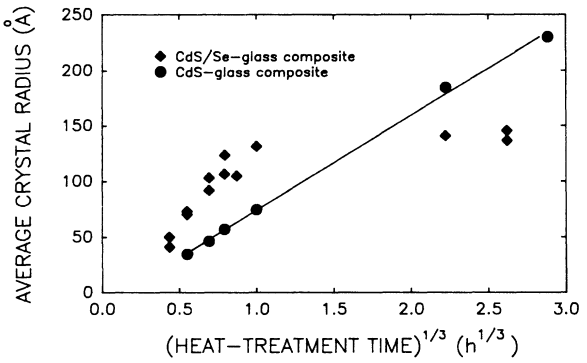

FIG. 3. Average crystallite radius dependence with the cube root of the heat-treatment time observed for CdS- and CdS_xSe_{1-x}-glass composites heat treated at 800 and 740 °C, respectively.

particles is unlikely. In a system exhibiting this effect, larger particles are unstable with respect to the degree of supersaturation and they grow by precipitation of solute from the matrix, while smaller particles, also unstable with respect to the solute concentration, dissolve back into the matrix. The precipitation rate dominates and the degree of supersaturation decreases, thereby leading to a time-dependent increase in the critical particle size which defines the boundary between growth and dissolution. Thus, as the process progresses, increasingly larger particles have radii below the critical size, causing them to shrink, which moves the average radius of stable grains to higher values.

Lifshitz and Slyozov[9,10] have developed a model for the diffusive decomposition of a supersaturated solid solution whose later stages, when the supersaturation has decreased sufficiently, yield a $t^{1/3}$ power-law behavior of the average size, R_{av}. (Although the following discussion assumes the coarsening grains to be spherical, Lifshitz and Slyozov state that incorporation of a nonspherical geometry should only change some numerical constants in the expressions found thus enabling their application to the present system.) The treatment stems from the Thomson-Freundlich relationship, which relates the curvatures of spherical grains to their corresponding activities and hence solubilities in solution, by the equation

$$RT \ln \frac{a_2}{a_1} = 2V_m \sigma \left[\frac{1}{r_2} - \frac{1}{r_1} \right] . \tag{1}$$

This equation defines the coarsening process as occurring when a condition of locally high solute concentration near the surface of high-curvature grains and lower concentration at the surface of larger-radius (low-curvature) particles sets up a concentration gradient which drives the diffusion of matter from the smaller to the larger particles. The resulting growth rate is expressed as

$$\frac{dR}{dt} = \frac{D}{R} \left[\Delta - \frac{\alpha}{R} \right] , \tag{2}$$

where D is the diffusion coefficient, R is the particle radius, Δ is the supersaturation, $\Delta = \bar{C} - C_\infty$, and $\alpha = 2V_m \sigma C_\infty / RT$; $\bar{C}$ is the average solute concentration and C_∞ is the equilibrium solubility. The critical radius is found as

$$R_{cr}(t) = \alpha / \Delta(t) . \tag{3}$$

Lifshitz-Slyozov's treatment of the process yields the often observed $t^{1/3}$ growth rate power law but the details of their predicted particle size distributions, however, are not often followed. This probably results from their assumption that the volume fraction of solute material is sufficiently small that the distance between coarsening particles is much greater than their radii. Voorhees and Glicksman,[11] in an elegant treatment of the more likely

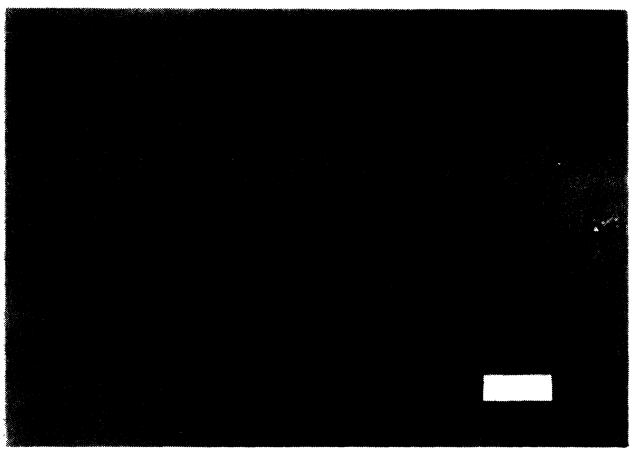

FIG. 2. Microstructure observed in TEM analysis of a CdS_xSe_{1-x}-glass composite subjected to a 20-min heat treatment at 740 °C (the bar represents 0.1 μm). (Note: the clustering of crystals evident here is an artifact of the sample extraction method and is not representative of actual morphology in the material.)

case of systems with higher fractions of solute particles, model interparticle diffusion effects during coarsening and show that the initial volume fraction significantly influences the final steady-state size distribution observed for the ensemble of particles.

The semiconductor-glass composite studied here only contains 0.5% CdS, therefore, despite a lack of volume fraction data, it was judged to be low and to satisfy the Lifshitz-Slyozov approximation. The treatment, using an asymptotic solution to the continuity and mass-conservation equations for the system, yields the expected result that at long times

$$R_{\rm av}^3(t)=R_{\rm cr}^3(t)=\tfrac{4}{9}D\alpha t \ . \tag{4}$$

While at shorter times, the time dependence of the critical and average sizes can be written as an expansion in $(\ln t')^2$ as follows:

$$x^3(t')\cong\tfrac{4}{9}t'\left[1+\frac{3}{4(\ln t')^2}(1+\cdots)\right], \tag{5}$$

where the reduced critical size is $x(t)=R_{\rm cr}(t)/R_{\rm cr,0}$; the reduced time is $t'=t/T-1$ and $T=R_{\rm cr,0}^3/\alpha D$. For the purpose of this discussion, the "diameter" of the CdS crystallite is taken to be their largest dimension while half this value is assumed to be their "radius."

The value of $R_{\rm cr,0}$ was taken to be the average particle "radius" for the shortest time distribution (5 min heat treatment); the product αD was obtained from the asymptotic behavior of $R_{\rm av}^3$, and the data thus reduced are plotted in Fig. 4 and are compared with the LS model, Eq. (5).

The Lifshitz-Slyozov treatment is further tested by comparison with the distribution of particle sizes developed after longer treatment times. The model predicts that the normalized distribution will follow:

$$P(u)=\begin{cases}\dfrac{3^4e}{2^{5/3}}\dfrac{u^2\exp[-1/(1-2u/3)]}{(u+3)^{7/3}(\frac{3}{2}-u)^{11/3}}, & u<1.5\\ 0, & u>1.5\ ,\end{cases} \tag{6}$$

where $u=R(t)/R_{\rm cr}(t)$. The reduced distribution data are plotted in Fig. 6 and compared to the LS formula, Eq. (6).

Both Figs. 4 and 5 show an excellent overall agreement between the data and the LS model. The initial critical radius $R_{\rm cr,0}$ was chosen as ~ 30 Å, obtained through the conviction that the five minute treatment equated an apparent induction time in the particle development, before growth could begin. This belief is supported by photoluminescence data which also indicate the presence of an induction period of about five minutes.

The data in Fig. 5 clearly show the characteristic vanishing of the distribution above $u=1.5$ as predicted by the model and the characteristic abrupt increase to a maximum near $u=1$. However, the data distribution is slightly broader and shows no continuous tail extending to $u=0$. This effect could be a result of the limited sampling and crystal gathering technique used in the TEM replication procedure. The measurements show a well-defined size cutoff, below which no crystal is measured. However, this cutoff value is not the same for all measurements and actually grows with heat-treatment time, also essentially as the $t^{1/3}$ power law. It is not evident at this time whether this cutoff is solely due to experimental technique, or is a result of an accelerated dissolution process, or is a combination of both.

In summary, the close adherence of the LS model to the crystal-growth data for the CdS-doped glass is strong evidence that, with heat treatment, the crystals grow by a strict diffusion-limited structure-coarsening process in which the composition remains unchanged and only the microstructure size of the particles changes with time. By contrast, the growth data from the mixed crystal glass shown in Fig. 3 is clear evidence that the process is not a pure coarsening process. The behavior depicted by Fig. 3 for the mixed-crystal glass appears to be most consistent with a gradual change in crystal stoichiometry associated with an increase in Se concentration with heat-treatment time resulting from a large difference in diffusion coefficient in the glass between sulfur and selenium ions.

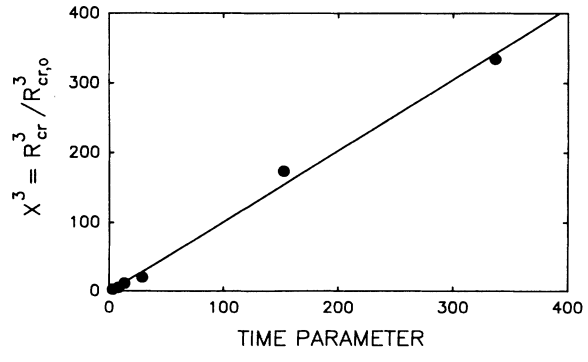

FIG. 4. The dimensionless critical radius behavior exhibited by the CdS-glass composites as a function of the time parameter [right-hand side of Eq. (5)] developed in the Lifshitz and Slyozov model.

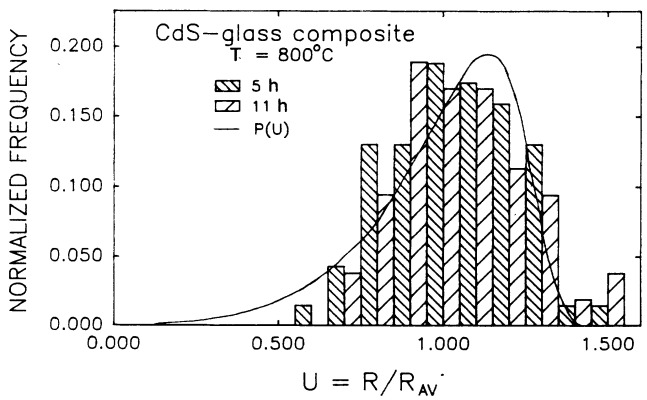

FIG. 5. Crystallite size histograms generated from CdS-containing samples heated for 5 and 11 h at 800 °C. The Lifshitz-Slyozov theoretical asymptotic size distribution has been included for comparison.

Optical characterization

Optical-absorption spectra collected at 9.0 K for the CdS-containing glasses heat-treated for various times at 800 °C are presented in Fig. 6. A slight shelf in the curves is visible at shorter times which shifts to longer wavelengths and develops into a peak separated from the main absorption plateau at longer heat-treatment times, as the crystallite size increases.

Photoluminescence data obtained for the same glass specimens exhibits a sharp peak in the blue with a broad luminescence band extending into the red. These two features are separated from each other by another broad band (see Fig. 7). The sharper, high-energy peak again exhibits a crystallite-size dependence moving upward in energy as the crystals decrease in size.

The PL peak and absorption shelf energies are plotted in Fig. 8 as a function of the inverse average crystallite size squared, the generally recognized functional parameter of interest in a quantum-confined system. A linear behavior is seen, indicative of a quantum size effect occurring to shift the energy of the underlying electronic state responsible for the optical features observed.

Insight into the identity of this state was obtained through Raman data collected from these specimens (details of which will be discussed in a forthcoming paper).[12] Resonance Raman (RR) LO-phonon harmonics up to the fourth order were found to occur indicating the existence of an intermediate state in the microcrystals. Enhancement of a particular order was exhibited when the sharper PL peak coincided with the Raman line position, analogous to the behavior seen in bulk CdS when the PL peak due to exciton-related recombinations appeared near an LO-phonon harmonic. In the bulk case, the exciton state was found to be responsible for the resonant effect, leading us to not only identify the state causing the sharp PL peak in the glass as the intermediate state responsible for the RR effect, but also to tentatively assign it an excitonlike origin.

Models explaining the confinement of charged particles in a three-dimensional potential well typically involve the

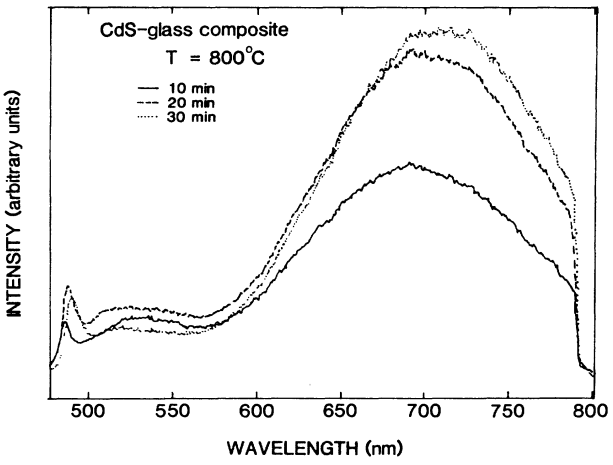

FIG. 7. Representative photoluminescence spectra collected at 9.0 K from CdS-glass composites heat treated at 800 °C for 10, 20, and 30 min.

solution of Schrödinger's wave equation using the Hamiltonian

$$H=\frac{-\hbar^2}{2m_e}\nabla_e^2-\frac{\hbar^2}{2m_h}\nabla_h^2+V_0\ . \tag{7}$$

Variation between treatments generally originates from differences in expressions assigned to V_0 which normally will contain the Coulombic interaction term. Boundary conditions are imposed forcing the wave functions describing the carriers to zero at the walls of the potential well.

Brus[13] has developed a model involving the confinement of an electron and hole within a dielectric sphere in a system where polarization-related terms incorporated into V_0 above contribute significantly to the kinetic energy of confinement and the Coulombic interaction energy. This treatment is valid, however, only for sizes where the kinetic energy of localization is larger

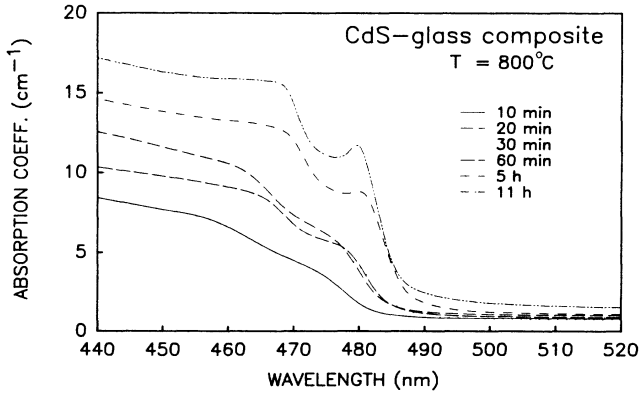

FIG. 6. Representative optical-absorption spectra collected at 9.0 K from CdS-glass composites subjected to increasing heat-treatment durations at 800 °C.

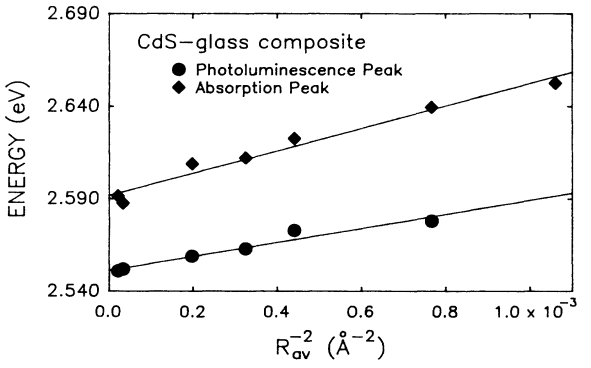

FIG. 8. Co-plot depicting the behavior of the 9.0-K absorption shelf and sharper PL peak energies for the CdS-containing specimens as a function of the inverse average square crystallite radius.

than the electrostatic energy. For larger spheres, the Coulomb-related correlation between the charged particles is handled through the use of a variational approach involving higher-order wave functions of the confined particles. These incorporate radial but not angular correlation between the electron and hole.

Efros and Efros[14] delineate the situation into three separate sphere-size regimes dependent upon the size of the dielectric sphere (R) and its relationship to the Bohr radii of the carriers (a_e and a_h). An interband-absorption threshold energy is then calculated through an evaluation of transition probabilities for the different regimes. The two extreme cases are shown as

$$\hbar\omega_0 = E_g + \frac{\hbar^2\pi^2}{2\mu R^2}, \quad \mu = \frac{1}{m_e} + \frac{1}{m_h}, \quad R < a_h < a_e \tag{8}$$

$$\hbar\omega_0 = E_g - E_{\text{ex}} + \frac{\hbar^2\pi^2}{2MR^2}, \quad M = m_e + m_n, \quad a_h < a_e < R \ . \tag{9}$$

The difference between these two cases resides in the relative contribution of energy components to the Hamiltonian. For small crystals [Eq. (8)] the kinetic energy of localization for the individual charge carriers is much greater than their Coulombic interaction. Conversely, the Coulombic interaction dominates in the case of large crystals [Eq. (9)] and the size confinement only affects the translational motion of the exciton as a unit or quasiparticle within the crystal.

Using the measured CdS bulk-carrier effective masses to obtain Bohr radii given by $\hbar^2\chi/(me^2)$ (where χ is the electronic susceptibility) it can be seen that, for the crystallite sizes found in the measurements reported here, the proper Efros and Efros size regime is the final one given above ($a_e = 15.9$ Å, $a_h = 3.8$ Å, and exciton Bohr radius $a_0 = 26.2$ Å).

Variational calculations performed by Kayanuma[15] and Nair *et al.*[16] to model the lowest electron-hole state in semiconductor spheres larger than the size of the bulk exciton show that significant energy shifts above the bulk free-exciton energy remain at sphere sizes many times the size of the Wannier exciton, presumably due to remaining confinement effects on the electron-hole wave functions. Although this is the region where the exciton is expected to be confined as a unit, the slope of the energy dependence on inverse size squared still yields effective-mass values less than bulk values in Nair *et al.*'s treatment.

Nair *et al.* show that the total-exciton-mass-confinement effect proposed by Efros and Efros is only appropriate at crystal sizes $R \geq 10a_0$ where the exciton might be expected to behave as a single particle. In the range between $a_0 \leq R \leq 10a_0$, they use a trial wave function

$$\Psi(\mathbf{r}_e, \mathbf{r}_h) = \begin{cases} N \left[\dfrac{\sin(\pi r_e/R)}{r_e/R} \right]^{\alpha_1} \left[\dfrac{\sin(\pi r_h/R)}{r_h/R} \right]^{\alpha_2} \exp(\beta r_{eh}/R), & \text{inside } R \\ 0, \quad \text{outside}, \quad r_{eh} = (\mathbf{r}_e - \mathbf{r}_h) \ , \end{cases} \tag{10}$$

with size-dependent variational parameters α_1, α_2, and β which they calculate for CdS in the size range 10–400 Å. The ground-state energy shift due to size confinement, resulting from this function, was calculated from their Fig. 1 for CdS.

The absorption threshold energy predicted by the two Efros and Efros limits at very small crystallite size (the effective mass equal to the reduced mass) and at very large crystallite size (the effective mass equal to the translational mass of the exciton) is plotted as a function of inverse square crystal radius along with the experimental absorption edge energy (taken to be the inflection point of the absorption curve at the initial absorption increase seen) in Fig. 9. The energy variation derived by Nair *et al.* is also shown for comparison. Immediately evident is the fact that the experimental data follows closely the behavior predicted for excitons whose translational motion alone is affected by the crystal size confinement. The slopes of the theoretical curves and the experimental data can be calculated to yield an effective mass corresponding to the various approaches used.

The derivative of the energy with respect to the inverse radius squared yields an effective mass which can be calculated from the data: $M_{\text{meas}} = 0.92m_0$. This can be compared to the excitonic translational mass of $M = m_e + m_h$, which ranges from $0.99m_0$ to $1.22m_0$, the reduced mass of $\mu = 0.15m_0$ and to a calculated effective mass of $0.30m_0$ for the Nair model.

The results therefore show that the variational calculation of Nair *et al.* gives a strong underestimate of the Coulomb coupling of the electron and hole ground-state energy at crystal sizes in the regime of $2a_0 \leq R \leq 15a_0$ covered by the data. In fact, the rigid particle model of Efros and Efros works very well and gives a close approximation of the experimental slope with an effective mass (translational mass) only about 10–30% larger than the experimentally derived mass. This indicates that the exciton exhibits a very strongly correlated electron-hole motion, down to crystal sizes as low as $R = 2a_0$.

An analysis of the optical behavior of CdS crystals in glass was also conducted by Ekimov and Onushchenko[20] and Ekimov *et al.*[21] over the range 12–400 Å. They observe three absorption oscillations at 4.2 and 300 K which they interpret as electronic transitions of the ground state and first two excited states. However, they analyze their results using the Efros and Efros model

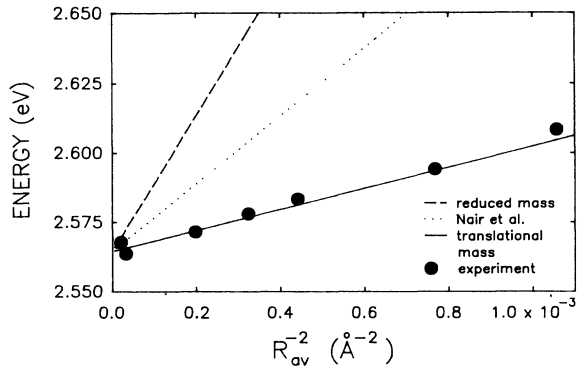

FIG. 9. The lowest excited-state energy plotted as a function of the inverse average square crystallite radius using the Efros and Efros first and third size regime interpretations and the variational approach of Nair *et al.* Experimentally observed absorption threshold energies are also included for the CdS-glass composites.

with the modification of neglecting the Coulomb interaction and ignoring the hole contribution to the shift in energy with size. By presuming that they are observing pure electronic transitions, they find good agreement between the slope of energy versus inverse square radius, and the free-electron effective mass. We find these results surprising since the observed absorption is more likely due to exciton transitions and the size range (40–400 Å) from which the slope measurements are taken falls in the region where the Coulomb interaction is known to be effective in determining the electron-hole orbits.

To allow for the size dispersion of crystals described by the Lifshitz-Slyozov asymptotic distribution, an additional constant factor is incorporated by Efros and Efros into the threshold absorption energy expressions. Use of the pertinent factor by Ekimov *et al.*[21] (for $a \ll a_e$ and $a \ll a_h$) results in a shift of the effective electron mass even closer to the expected bulk value. Use of this factor in the present analysis results in an experimental mass term $\sim 32\%$ smaller than has been reported here, thus indicating a lesser degree of electron-hole correlation or a greater modification of the internal, orbital motion.

The work of Ekimov *et al.*[17] and Ekimov and Onushchenko[18,19] with $CuCl_2$ showed that in those crystals, the effective mass calculated from the data was intermediate between the reduced mass (uncorrelated motion) and the translational mass (rigid particle motion). The treatment by Nair *et al.* added sufficient coupling to the electron-hole behavior to better fit the $CuCl_2$ data in the size regime above $R = 2a_0$. But our data on CdS clearly show that their treatment underestimates the Coulomb interaction at sizes in the same relative range ($2a_0 \leq R \leq 15a_0$). This result thus shows that the size confinement effect measured in CdS results primarily from a limit on the translational behavior of the exciton and that any modification of the internal orbital motions of the electron and hole are relatively small. Our studies were able to reduce the average crystal radius to only ~ 30 Å. While they clearly show the size dependence of the quantum confinement effect, it would be instructive to reduce the crystal size below the exciton radius to see if the effective mass decreases as the average radius approaches a_0. However, it seems clear from our data that the CdS crystals are nucleating from the glass matrix at a critical nucleus of about 20 Å radius, and that a further reduction in radius is not thermodynamically possible. A new fabrication initiative is underway to make samples with a smaller interface energy difference, and consequently a smaller critical nucleus, by changing the host glass.

CONCLUSIONS

The study of quantum confinement effects on the energy levels of excitons in semiconductors has been plagued mostly by substitutional alloying effects which also alter the band-gap energy of semiconductors. In the study presented, we have conducted a detailed analysis of the crystal growth of CdS and CdS_xSe_{1-x} semiconductors in a glass matrix. The results showed that only the CdS composite allowed the crystals to grow without an associated change in their composition. The CdS crystals were shown to grow from a critical nucleus to large sizes by strictly following a diffusion-limited particle coarsening process modeled by Lifshitz and Slyozov. Therefore, it was concluded that to satisfy the conditions of the model, the particles grew from a supersaturated solution *without* a change in composition of the particles. In contrast, similar studies of glass containing CdS_xSe_{1-x} crystals showed that a time-dependent alloying process associated with the crystal growth is likely. This process appears to result from a difference in interdiffusion coefficient between the sulfur and selenium ions in the glass. This interpretation is indirectly supported by optical-absorption edge and blue photoluminescence measurements which show an unexpectedly large decrease in exciton binding energy with crystal growth at short heat-treatment times.

Optical studies of the CdS crystals at sizes between 40 and 400 Å showed a clear inverse square size dependence in both the absorption edge and the photoluminescence peak at room temperature and at 9 K. The PL peak was associated with an exciton recombination process (most likely a Wannier exciton) by the study of the shift in amplitude of the higher orders of resonant LO-phonon Raman scattering peaks, as these harmonics were tuned to the photoluminescence emission.

The dependence of the absorption edge on crystal size was analyzed with the models of Efros and Efros and of Nair *et al.* The data show that even at sizes as low as $2a_0$, the quantum size effect does not significantly modify the internal structure of the exciton and the absorption data yields an effective mass only about 10–30% lower than the exciton translational mass predicted by Efros and Efros. In no size range does the data exhibit as low an effective mass as predicted by the Nair-Sinha-Rustagi (NSR) model, which treats the effect of the boundary on the internal electron-hole orbits by using a variational method to include the Coulomb potential effect on the system confined in a spherical potential well.

The data show that the effect of the Coulomb interaction is strongly underestimated in the NSR model and

that for the system studied, the translational confinement model adequately describes the effect of the reduced semiconductor size with possibly a small modification due to a confinement effect on the electron and hole wave functions.

Quantum confinement effects in semiconductors of small sizes are of great interest since they can lead to an understanding of the interplay of the fundamental interactions of electrons and holes and the effect of boundaries or surfaces. In semiconductor-glass composites, the glass phase appears to only play the role of an infinite potential barrier and, therefore, these systems are of interest for modeling studies. These quantum confinement effects have a variety of applications since they can lead to an increase in the exciton binding energy of selected semiconductors sufficient to allow the excitonic levels to remain distinct at higher temperatures. This phenomenon is presently of great interest for nonlinear optical processes which utilize resonant exciton transitions and state-filling effects to induce a large rapid change in the refractive index of the crystal with a subnanosecond decay time. The glasses, studied here, have great promise in this area. CdS single crystals have exhibited low-temperature, excitonic nonlinearity,[22] and semiconductor-glass composites, similar to those studied here, have shown carrier plasma nonlinearities at room temperatures.[23]

ACKNOWLEDGMENTS

The authors are indebted to Mr. Lee Cook, currently at Galileo Electro-Optics Laboratories, for supplying them with the samples and for guidance regarding the phase instabilities of the glasses studied. The authors are also indebted to the Air Force Office of Scientific Research for their support of this work under Grant No. AFOSR-84-0395.

[1]J. Warnock and D. D. Awschalom, Phys. Rev. B **32**, 5529 (1985).
[2]J. Warnock and D. D. Awschalom, Appl. Phys. Lett. **48**, 425 (1986).
[3]N. F. Borrelli, D. W. Hall, H. J. Holland, and D. W. Smith, J. Appl. Phys. **61**, 5399 (1987).
[4]L. E. Brus, J. Chem. Phys. **79**, 5566 (1983).
[5]L. E. Brus, J. Lumin. **31&32**, 381 (1984).
[6]L. E. Brus, IEEE J. Quantum Electron. **QE-22**, 1909 (1986).
[7]R. Rossetti, S. Nakahara, and L. E. Brus, J. Chem. Phys. **79**, 1086 (1983).
[8]R. Rossetti, J. L. Ellison, J. M. Gibson, and L. E. Brus, J. Chem. Phys. **80**, 4464 (1984).
[9]I. M. Lifshitz and V. V. Slyozov, Zh. Eksp. Teor. Fiz. **35**, 479 (1958) [Sov. Phys.—JETP **35**, 331 (1959)].
[10]I. M. Lifshitz and V. V. Slyozov, J. Phys. Chem. **19**, 35 (1961).
[11]P. W. Voorhees and M. E. Glicksman, Acta Metall. **32**, 2013 (1984).
[12]B. G. Potter, Jr. and J. H. Simmons (unpublished).
[13]L. E. Brus, J. Chem. Phys. **80**, 4403 (1984).
[14]Al. L. Efros and A. L. Efros, Fiz. Tekh. Poluprovodn. **16**, 1209 (1982) [Sov. Phys.—Semicond. **16**, 772 (1982)].
[15]Y. Kayanuma, Solid State Commun. **59**, 405 (1986).
[16]S. V. Nair, S. Sinha, and K. C. Rustagi, Phys. Rev. B **35**, 4098 (1987).
[17]A. I. Ekimov, A. A. Onushchenko, A. G. Plyukhin, and Al. L. Efros, Zh. Eksp. Teor. Fiz. **88**, 1490 (1985) [Sov. Phys.—JETP **61**, 891 (1985)].
[18]A. I. Ekimov and A. A. Onushchenko, Pis'ma Zh. Eksp. Teor. Fiz. **34**, 363 (1981) [JETP Lett. **34**, 345 (1981)].
[19]A. I. Ekimov and A. A. Onushchenko, Fiz. Tekh. Poluprovodn. **16**, 1215 (1982) [Sov. Phys.—Semicond. **16**, 775 (1982)].
[20]A. I. Ekimov and A. A. Onushchenko, Pis'ma Zh. Eksp. Teor. Fiz. **40**, 337 (1984) [JETP Lett. **40**, 1136 (1984)].
[21]A. I. Ekimov, Al. L. Efros, and A. A. Onushchenko, Solid State Commun. **56**, 921 (1985).
[22]M. Dagenais and W. F. Sharfin, Appl. Phys. Lett. **46**, 230 (1985).
[23]R. K. Jain and R. C. Lind, J. Opt. Soc. Am. **73**, 647 (1983).

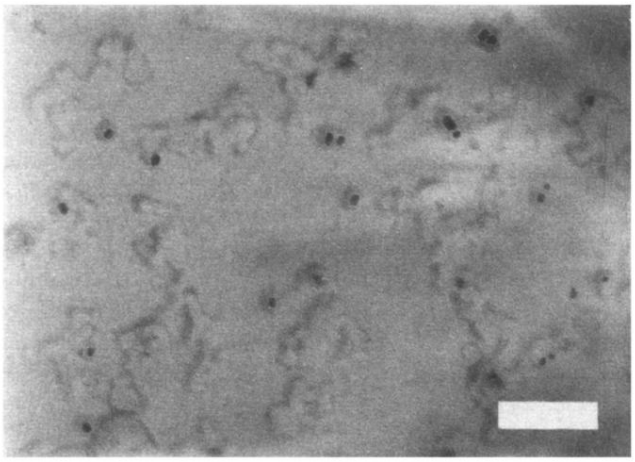

FIG. 1. Microstructure observed in TEM analysis of a CdS-glass composite subjected to a 20-min heat treatment at 800 °C (the bar represents 0.1 μm).

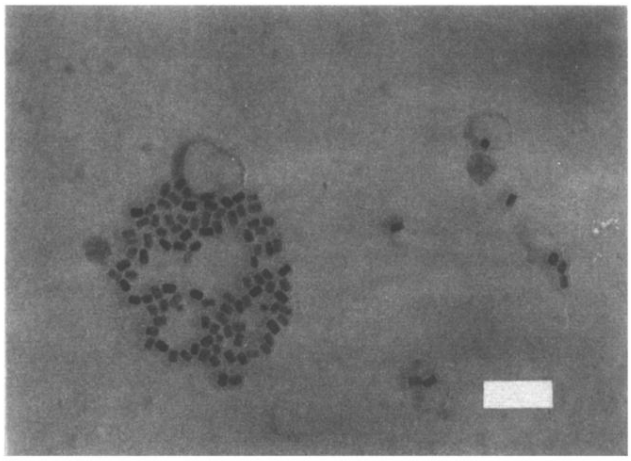

FIG. 2. Microstructure observed in TEM analysis of a CdS_xSe_{1-x}-glass composite subjected to a 20-min heat treatment at 740 °C (the bar represents 0.1 μm). (Note: the clustering of crystals evident here is an artifact of the sample extraction method and is not representative of actual morphology in the material.)